Supporting Information

Few-layer graphene as an efficient buffer for epitaxy of GaN/AlN on SiO₂/Si substrate: combined experimental and theoretical study

D. P. Borisenko[1,*], A. S. Gusev[1,*], N. I. Kargin[1], P. L. Dobrokhotov[1], A. A. Timofeev[1], V. A. Labunov[1,2], M. M. Mikhalik[2], K. P. Katin[1,*], M. M. Maslov[1], P. S. Dzhumaev[1] and I. V. Komissarov[2]
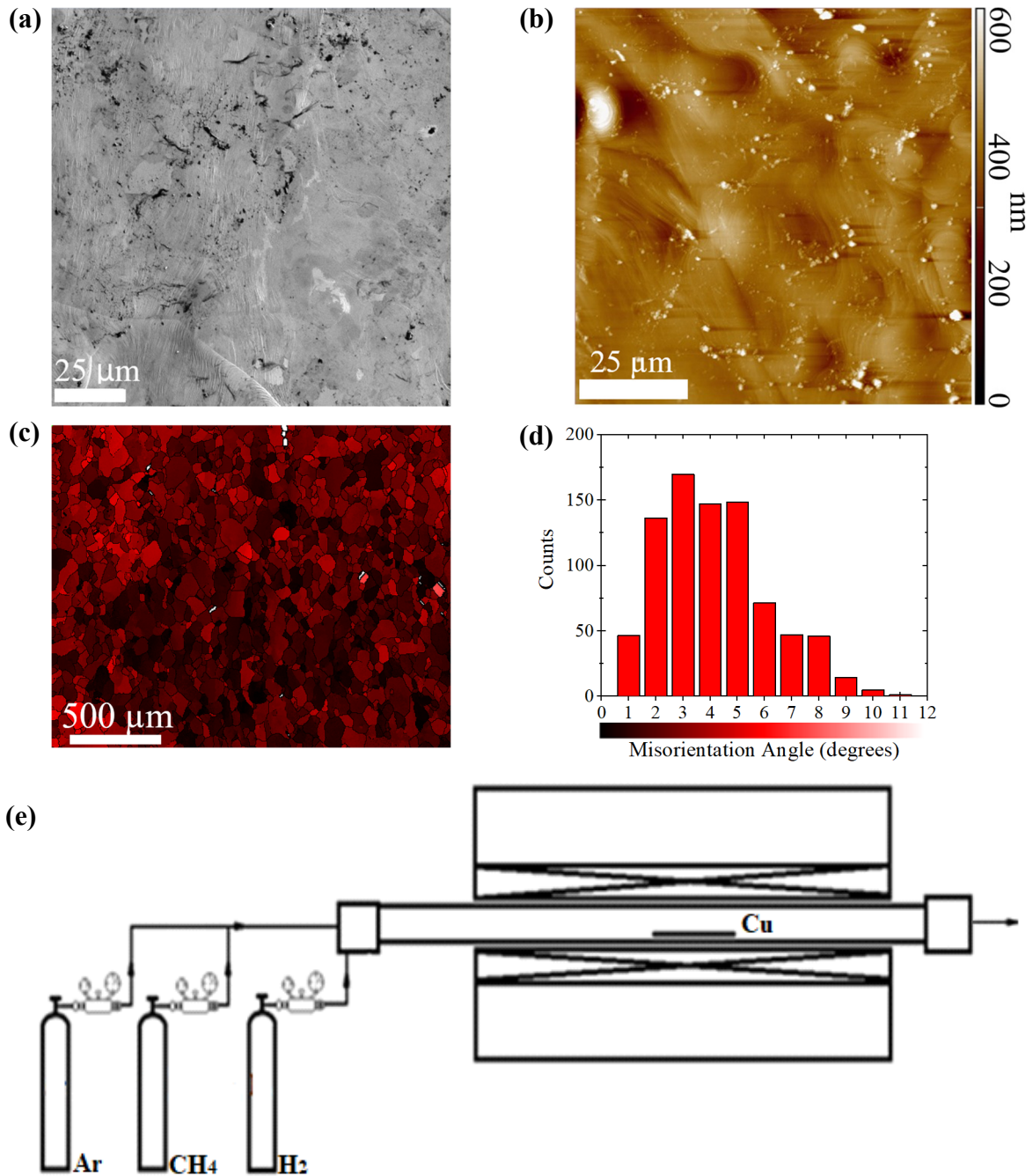
[1]National Research Nuclear University MEPhI, 115409 Moscow, Russia

[2]Belarusian State University of Informatics and Radioelectronics, 220013 Minsk, Belarus

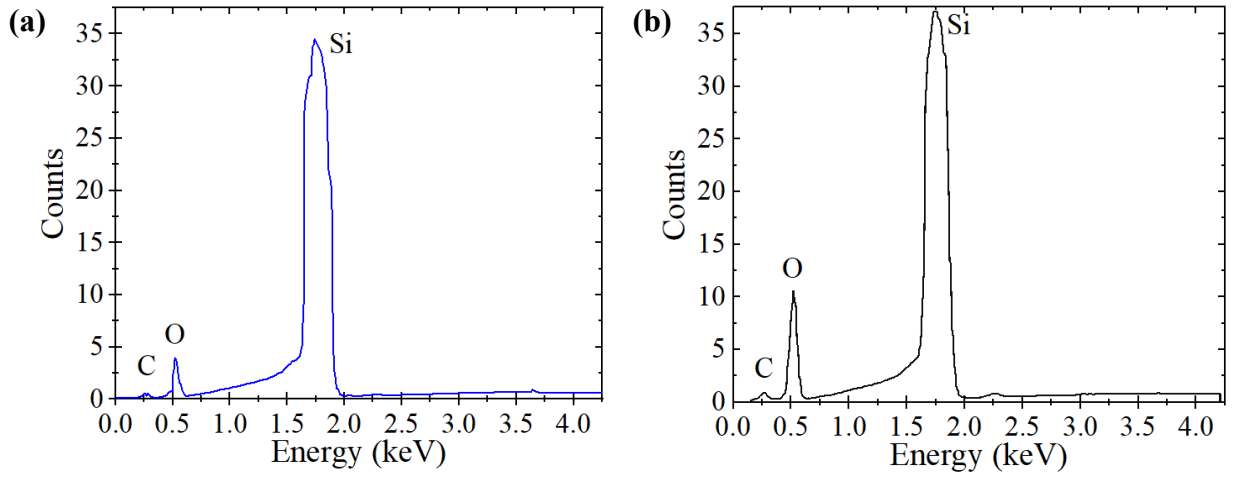* Correspondence: dpborisenko@mephi.ru (D.P.B.); asgusev@mephi.ru (A.S.G.); kpkatin@mephi.ru (K.P.K.)

S-I. EBSD analysis of the Cu foil after graphene growth.

SEM and AFM images on Figure S1(**a, b**) demonstrate a smooth surface of the copper foil without contamination, holes or cracks. Such surface quality contributes to the preparation of high-quality graphene.

Figure S1. (**a, b**) SEM and AFM images of the 25 μm Cu foil after graphene growth. (**c, d**) EBSD analysis of the Cu foil after graphene growth: (**c**) the orientation map of the angle deviation of the direction <100> of copper grains from the rolling direction; (**d**) the distribution of the misorientation angles for copper grains; (**e**) schematic diagram of the custom-made CVD setup.
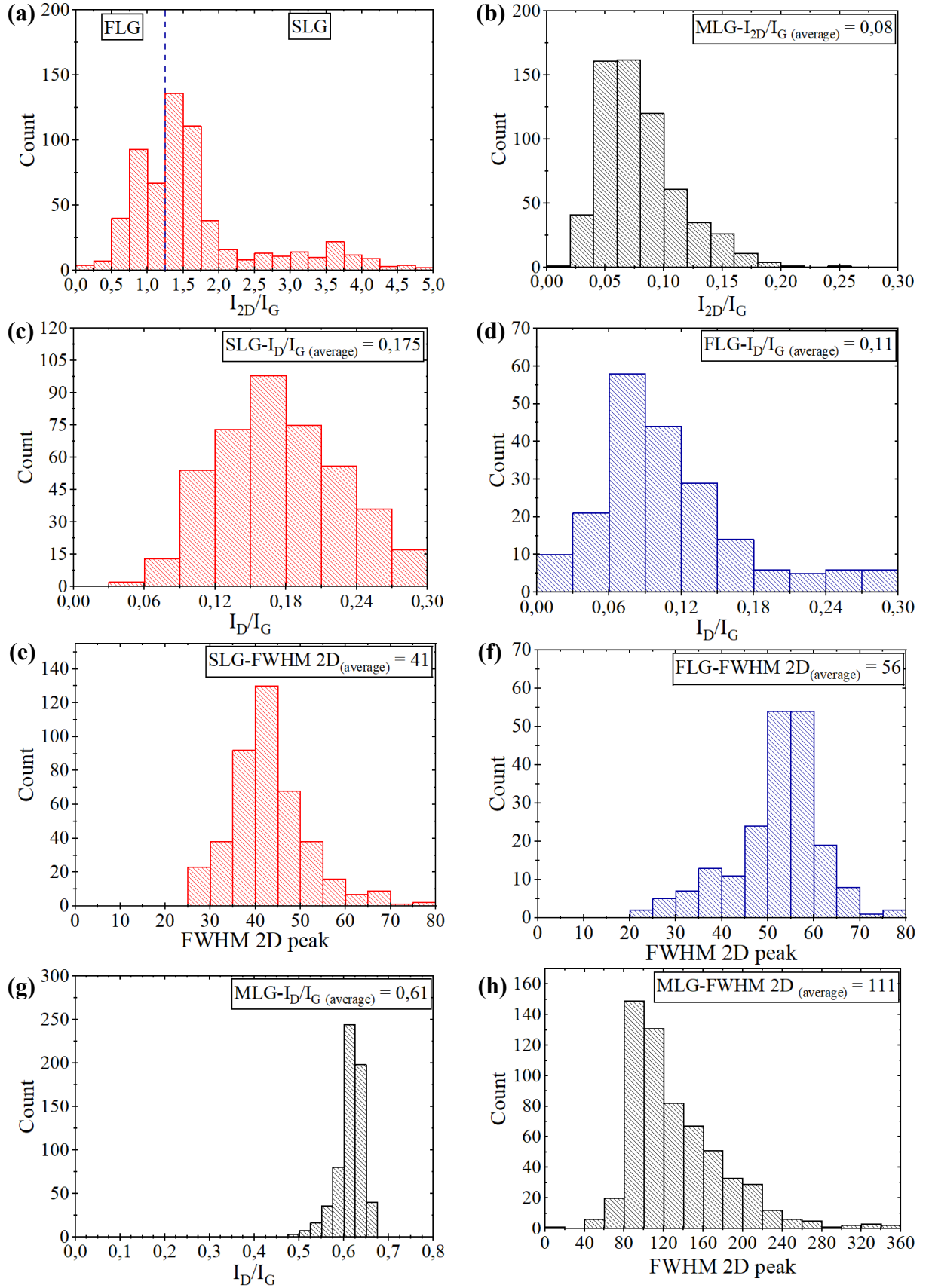
S-II. The EDX analysis for FLG and MLG on SiO$_2$/Si before nitrides PA-MBE growth.

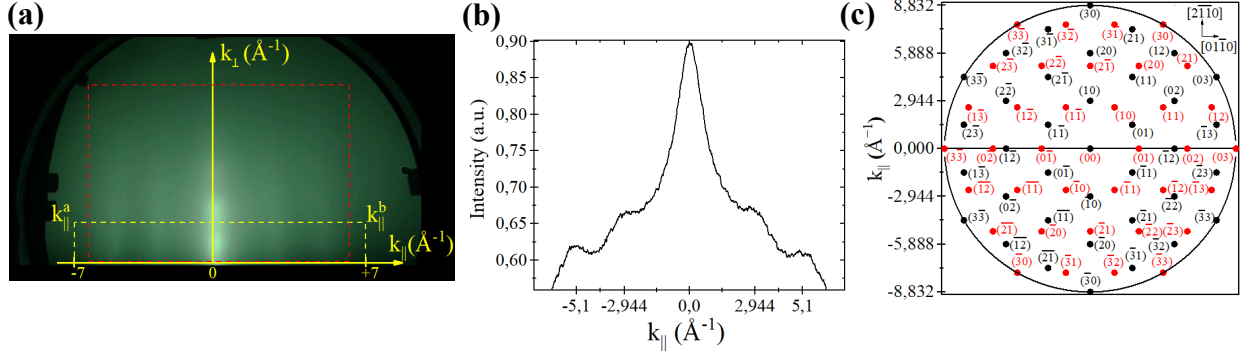**Figure S2.** EDX spectra of the FLG (**a**) and MLG (**b**).

Figure S2 shows EDX Spectra from random areas of FLG (Figure S2 (**a**)) and MLG (Figure S2(**b**)). In both cases, only three chemical elements were recorded: carbon (C), oxygen (O) and silicon (Si). The differences between FLG and MLG consists only in the percentage ratios of these elements.

S-III. Raman histograms for graphene on SiO_2/Si substrates.

Figure S3. Statistical histograms of the I_{2D}/I_G (**a, b**), I_D/I_G ratios (**c, d, g**) and 2D peak FWHM (**e, f, h**) measured from Raman spectra for SLG (**a, c, e**), FLG (**a, d, f**) and MLG (**b, g, h**) transferred onto SiO_2/Si substrates.

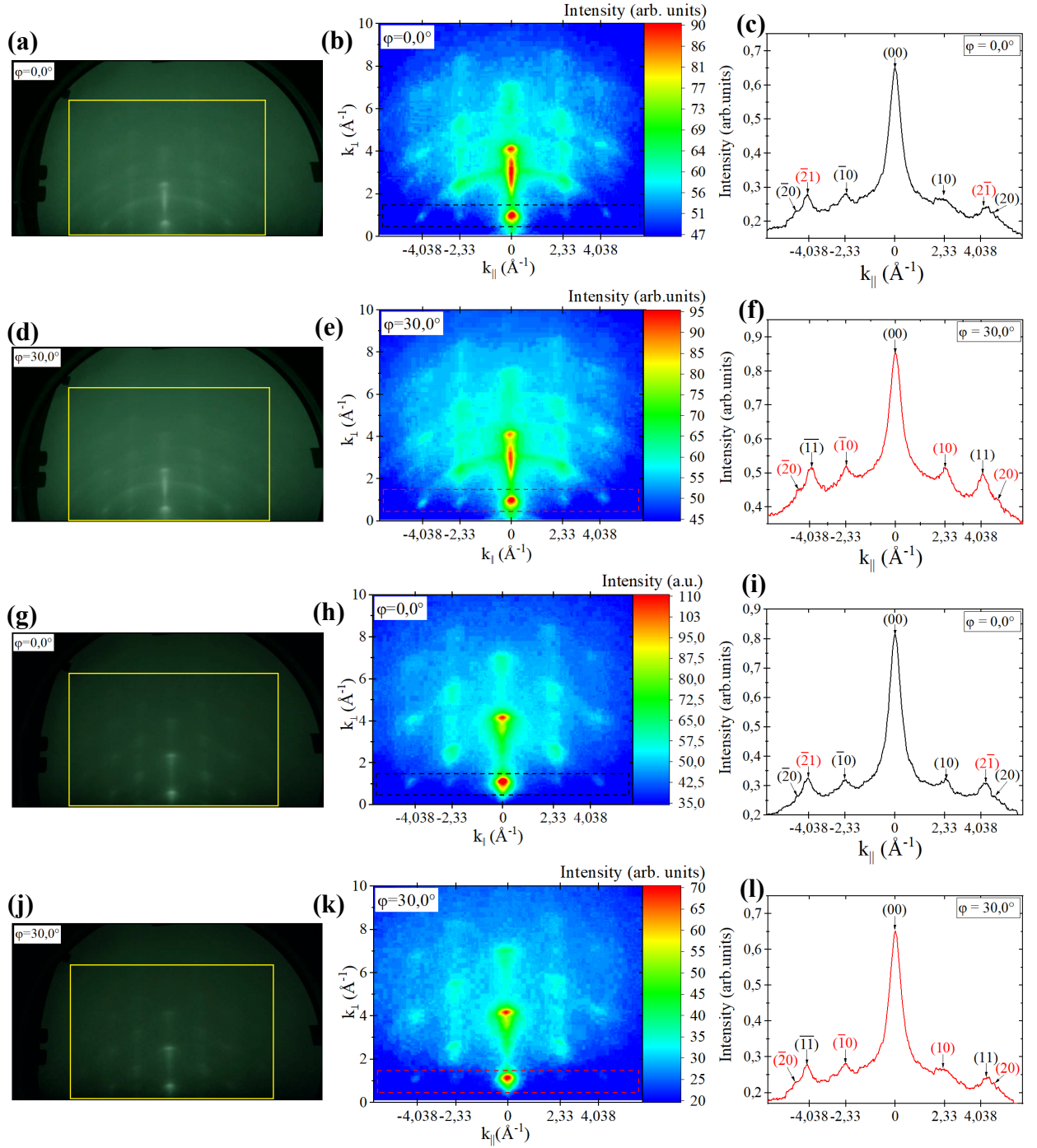## S-IV. RHEED methodology.

(a)

(b)

(c)

Figure S4. (a) A standard RHEED patterns collected from graphene sample with the 15 keV electron beam incident at $\varphi = 0°$. **(b)** Typical intensity profile along the $k_{\parallel}$ axis for graphene on SiO_2/Si substrate. **(c)** The theoretical 2D reciprocal space structure of the dual-domain graphene (the red spots are rotated 30° from the black spots around the $k_{\perp}$ axis).

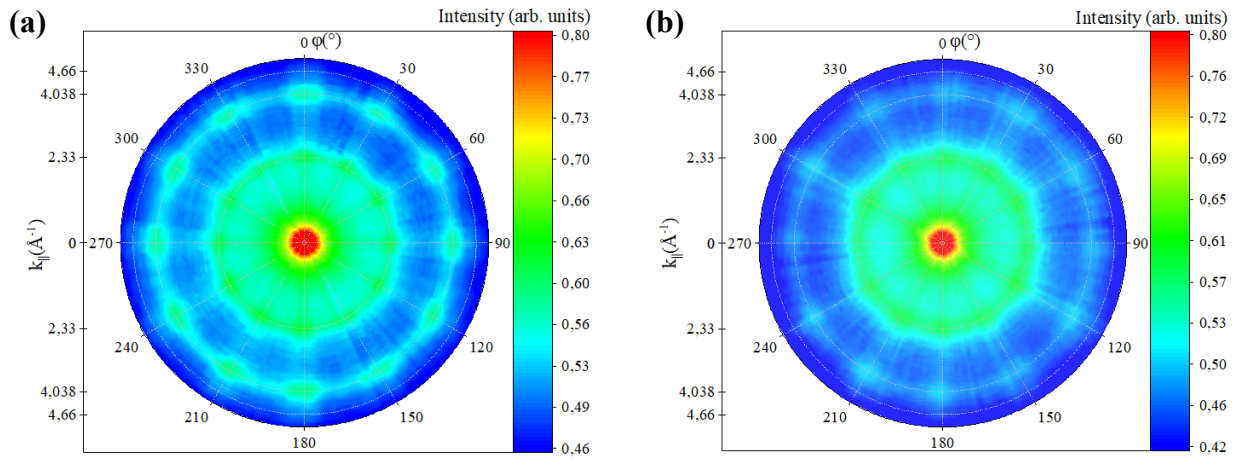The labeled positions $k_{\parallel}^a$ and $k_{\parallel}^b$ in Figure S4 **(a, b)** are chosen to be −7.0 Å^{-1} and 7.0 Å^{-1}, respectively. With each fixed value φ, the intensity profile I_{φ} $(k_{\parallel})$ was analyzed, similar to the shown in Figure S4**(b)**. In the case of the profiles analysis, the intensity was integrated along the direction $k_{\perp}$ (the area in the RHEED image (Figure S4**(a)**), highlighted by the yellow dashed line) to improve the signal-to-noise ratio. In addition to the original result (Figure 4**(a, d)** and Figure 5**(a, d)**), RHEED images were programmatically analyzed in order to obtain a clearer picture of the main peaks positions for the 2D reciprocal space structures of the studied samples (the region in the RHEED image (Figure S4**(a)**), highlighted by the red dashed line). By constructing azimuthally dependent intensity I_{φ} $(k_{\parallel})$ in the system of polar coordinates with a radius, which is $k_{\parallel}$ and a polar angle φ, and representing the intensity of various colors, 2D reciprocal space structures for graphene and nitrides samples were constructed.

The central streak represents the (00) point of the graphene reciprocal lattice. To facilitate understanding of the experimental results presented in this work, we present an indexed fragment of the reciprocal lattice of crystalline graphene domains, disoriented by 30°, with the location of the main peaks (Figure S4**(c)**). The red spots are the 2D reciprocal lattice points of single crystal graphene and the black spots are rotated 30° from the red spots around the $k_{\perp}$ axis.
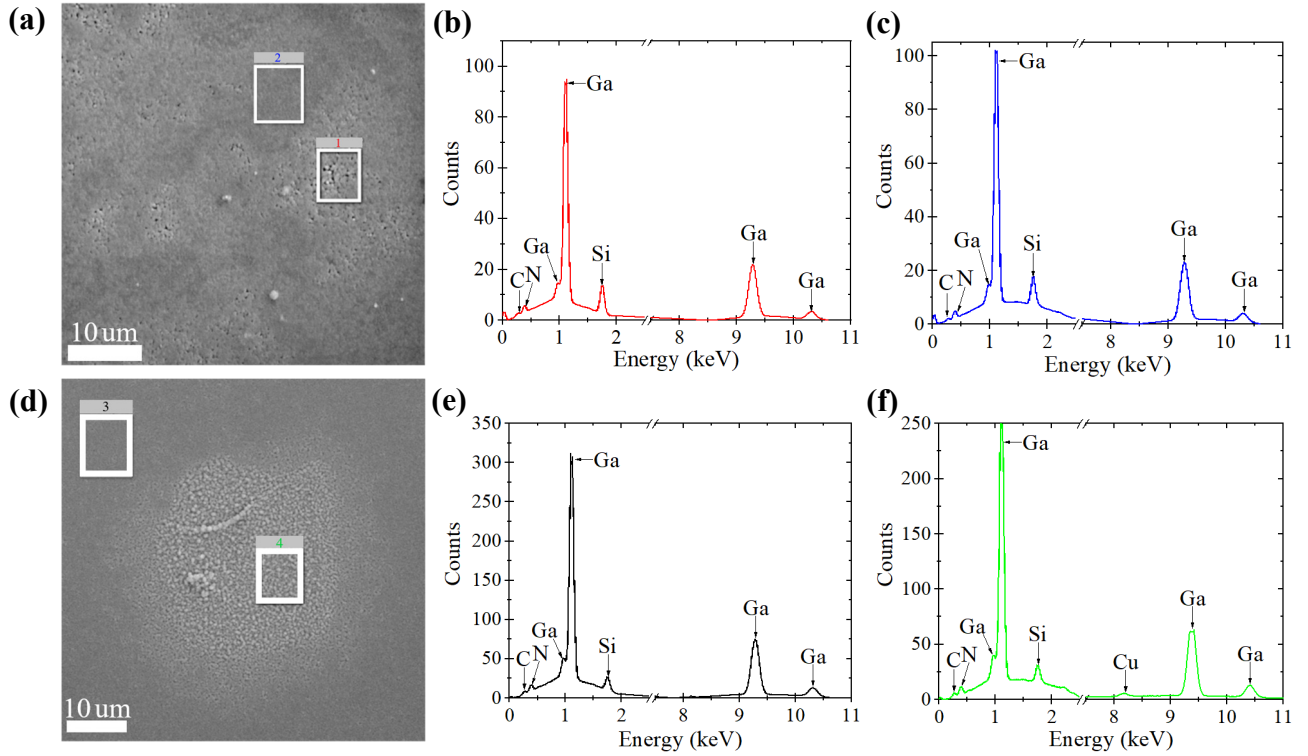
S-V. AlN nucleation process.

Figure S5.1. Real and programmatically processed images of RHEED patterns from AlN surface during PA-MBE growth on FLG (**a, b, d, e**) and MLG (**g, h, j, k**) at azimuthal angles φ = 0° (**a, b, g, h**) and 30° (**d, e, j, k**), respectively. Intensity profiles for azimuthal angles φ = 0° (**c, i**) and 30° (**f, l**) for AlN growing on FLG (**c, f**) and MLG (**i, l**), respectively.
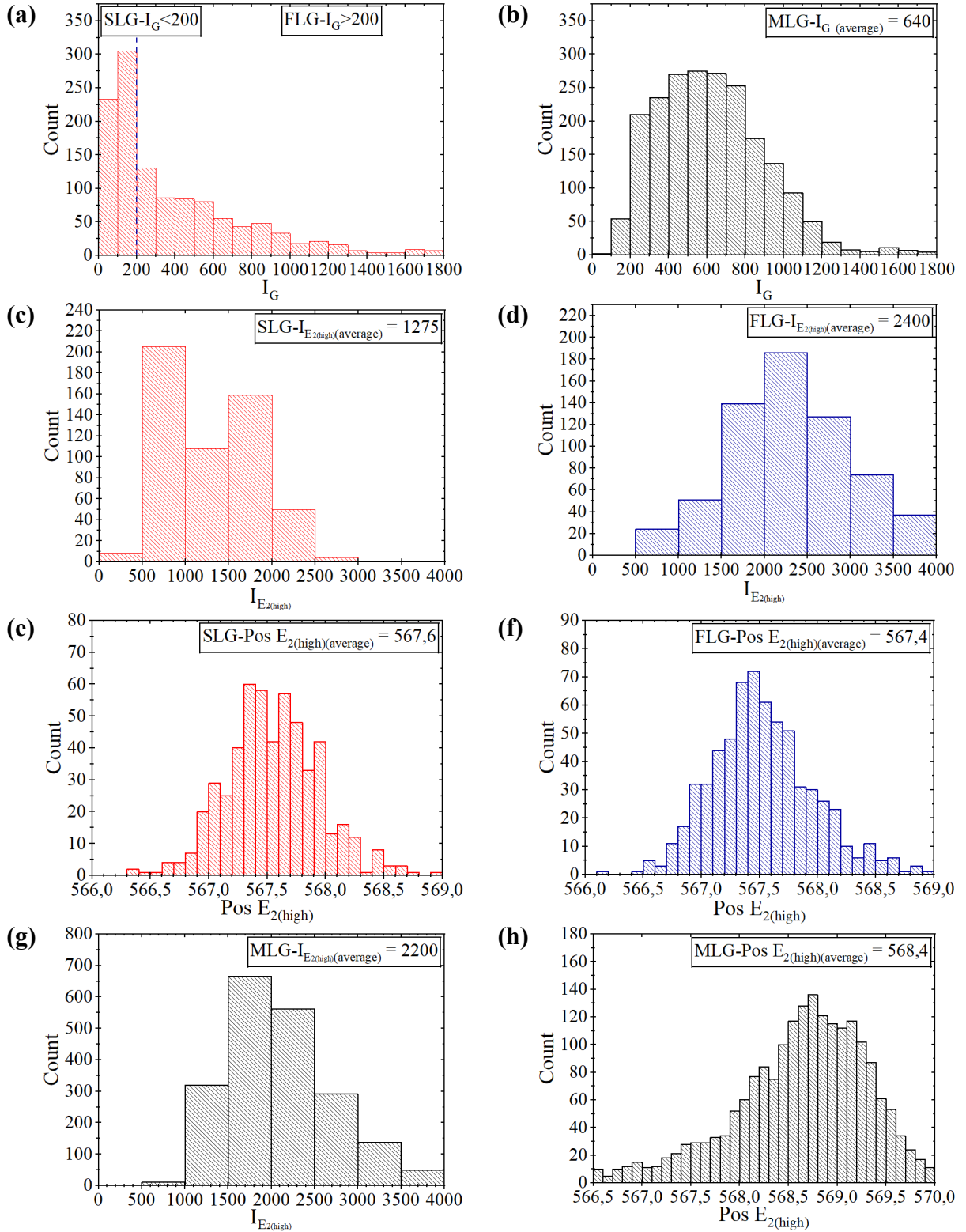
Figure S 5.2. (a, b) The RHEED reciprocal space structures for the AlN grown over the FLG **(a)** and MLG **(b)** buffer layers.

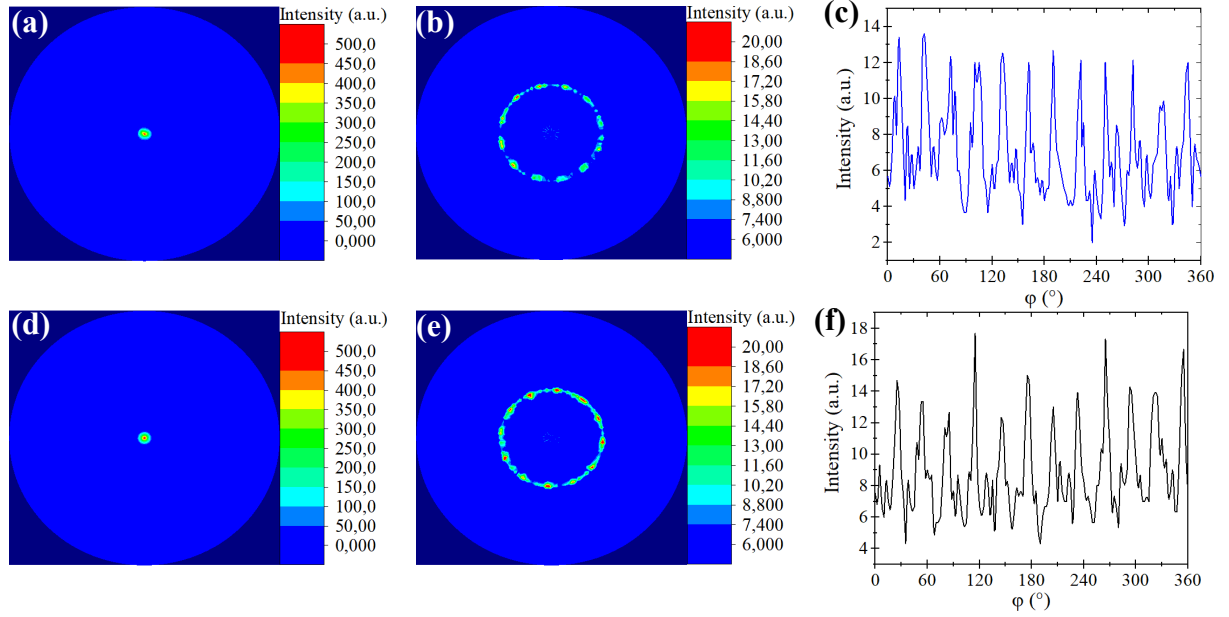## S-VI. The EDX analysis after nitrides PA-MBE growth.

Figure S6. SEM images of GaN/AlN grown on SLG-FLG **(a)** and MLG **(d)**. The EDX analysis for nitride grown on the SLG **(b)**, FLG **(c)** and MLG **(e, f)** buffers. **(f)** EDX Spectrum from GaN/AlN grown on the MLG in a region with a bubble.

S-VII. Raman maps and histograms for graphene and nitride after PA-MBE growth.

Figure S7. Statistical histograms of the I_G (**a, b**), $I_{E2(high)}$ (**c, d, g**) and position of $E_{2(high)}$ peak (**e, f, h**) measured from Raman spectra for SLG (**a, c, e**), FLG (**a, d, f**) and MLG (**b, g, h**) after PA-MBE growth.

S-VIII. XRD pole figures for GaN/AlN (0001) and GaN/AlN (10$\bar{1}$3).

Figure S8. The measured XRD pole figures for GaN/AlN (0002) (**a, d**) and GaN/AlN (10$\bar{1}$3) (**b, e**) films grown on the SLG (**a, b**) and MLG (**d, e**). The azimuthal scans of the XRD intensity (**c, f**) for GaN/AlN (10$\bar{1}$3) pole figures.

The texture of the GaN/AlN films was characterized by XRD pole figures (0002) taken at $2\theta = 34.6°$ and (10$\bar{1}$3) taken at 63.5° which are presented in Figure S8. The (0002) (Figure S8 (a, d)) and (10$\bar{1}$3) (Figure S8 (b, e)) XRD pole figures indicates the good c-axis orientation of the GaN/AlN film. On Figure S8 (c, f) azimuthal intensity distribution is shown at radial angle $\chi = 35°$ on (10$\bar{1}$3) pole figure (a ring with peaks on (10$\bar{1}$3) pole figure). This distribution demonstrates that there are actually 12 peaks with different intensity, confirming the presence of two types of domains with a 30° rotation with respect to each other. GaN/AlN layers are monocrystalline oriented in the (0002) direction and free of filamentous dislocations (Figure S8).